4-1-2022

Speed of Sound for Hadronic and Quark Phases in a Magnetic Field

Efrain J. Ferrer
The University of Texas Rio Grande Valley

A. Hackebill
CUNY Graduate Center

Speed of Sound for Hadronic and Quark Phases in a Magnetic Field

E. J. Ferrer and A. Hackebill
Dept. of Physics and Astronomy, University of Texas Rio Grande Valley, Edinburg 78539, USA, Physics Department, CUNY-Graduate Center, New York 10314, USA

(Dated: April 1, 2022)

It is well known that for a fermion system with an isotropic equation of state (EOS), the square of the speed of sound $(\mathrm{SOS})^2$ is a measure of the stiffness of the equation of state (EOS). It is also known that in the presence of a magnetic field the EOS becomes anisotropic with two different pressures arising, one directed parallel to the field direction and one perpendicular to it. Since the SOS in a medium is created by pressure oscillations, the anisotropy in the pressure should be transferred to the SOS. In this paper, we derive from first principles the anisotropic wavelike equation from where the expressions for the longitudinal and transverse SOS in the presence of a uniform magnetic field can be obtained. We also investigate the degree to which the magnetic field in the weak and the strong limit affects the two SOS of (i) a system of hadrons modeled by the nonlinear Walecka model and (ii) a system of quarks modeled by the MIT bag model. We find that for the systems considered, the effects of the magnetic field on the SOS anisotropy are mild up to 10^{18}G. Links to neutrons star physics are discussed throughout the paper.

PACS numbers: 26.60.-c,64.30.+t,13.40.Em,03.65.Vf, 12.39.-x

I. INTRODUCTION

Studies of matter under the extreme conditions of high temperatures and/or density are topics of increasing general interest in the physics community due to their significance for heavy-ion-collision experiments and for the astrophysics of compact objects. In both contexts, moreover, the presence of strong magnetic fields is undeniable. In this regard, we have that according to several numerical simulations, off-central Au-Au collisions at RHIC can lead to field strengths of 10^{18} - 10^{19} G, while the field can be as large as 10^{20} G for the off-central Pb-Pb collisions at the LHC [1]. On the other hand, neutron stars (NS) also exhibit significant strong magnetic fields. The surface magnetic fields of some radio pulsars are of order $10^{13} - 10^{14}$ G [2]. There are even some special compact objects called magnetars [3] whose surface magnetic fields are of order $10^{14} - 10^{15}$ G, which have been inferred from spectroscopic and spin-down studies of soft-gamma ray repeaters (SGRs) and anomalous x-ray pulsars (AXPs). In addition, we should take into account that the inner core magnetic fields of magnetars can be even larger, which follows from the magnetic field flux conservation in stellar media with very large electric conductivities. The inner fields have been estimated to range from 10^{18} G for nuclear matter stars [4] to 10^{20} G for quark matter stars [5]. The fact that strong magnetic fields populate the vast majority of astrophysical compact objects and that they have significant consequences for several star properties has motivated many works focused on the study of the EOS of magnetized NS (see [6] and references there). These strong magnetic fields, produced during the first instants after a collision or in the interior of NS, can create the conditions for observable QCD effects [7]. These effects can be prominent because the magnetic fields generated are of the order of or higher than the QCD scale, $eB > \Lambda_{QCD}^2$.

Regarding NS, despite an extended observational and theoretical effort carried out in recent years to determine the state of the extremely high-dense nuclear-star matter existing in its interior, this still remains an open question to be answered. The physics of matter at densities beyond nuclear density, $\rho_0 = 2.3\times10^{17} kg/m^3$, is a big challenge to theorists, with observations of NS being crucial for determining the correct dense-matter model. In this regard, recent very precise mass measurements of two compact objects, PSR J1614-2230 and PSR J0348+0432 with $M = 1.908 \pm 0.016 M_\odot$ [8] and $M = 2.01 \pm 0.04 M_\odot$ [9], respectively, where $M_\odot$ is the solar mass, have provided some constraints

on the interior composition of NS. These high mass values imply that the equation of state (EOS) of the corresponding stellar medium should be rather stiff at high densities. On the other hand, the recent detection of gravitational waves produced by the binary NS merger event GW170817 [10], has become also crucial for shedding new light on the internal structure of NS. For instance, it has been shown already [11] that strange stars with an inner phase of color superconducting quark matter is compatible with the deformability parameter space obtained from the GW170817 data [12]. These events will surely open the possibility for new advances in the determination of the compact-star EOS in the near future. It should be taken into account that binary neutron star mergers could be a common source, with an expected detection rate of ≈ 40 yr^{-1}, as predicted by population-synthesis models [13].

Another quantity that can shed also some light on the characteristics of the stellar inner matter is the speed of sound (SOS) V_s. This quantity is associated with how stiff the EOS is and consequently with how big the star's mass can be at a given radius. Causality imposes the absolute bound $V_s \leqslant c$ (From now on we will work in natural units with $c = 1$); but its value can be even more constrained. In an isotropic medium the SOS can be obtained from

$$V_s^2 = \frac{\partial P}{\partial \epsilon} \tag{1}$$

with ϵ the system energy density and P the pressure. Then, for incompressible matter the trace of the stress-energy tensor is constant

$$T = \epsilon + 3P = constant \tag{2}$$

from which the so-called conformal limit follows

$$V_s^2 = 1/3 \tag{3}$$

In lattice QCD calculations at finite temperature and zero chemical potential, and even at small baryonic chemical potentials, it has been obtained that $V_s^2 < 1/3$ [14]. But, the discussion of an upper limit to the speed of sound in NS goes back for some time [15]. More recently, SOS larger than the conformal limit has been reported for QCD at large isospin density [16], in two-color QCD [17] in holographic approaches [18], in resumed perturbation theory [19], in chiral effective field theory [20], in quarkyonic matter [21] and in models of high-density QCD [22]. A final answer to this important question regarding the maximum speed of sound allowed in dense quark matter might be answered by future astrophysical observations.

In this direction, observations of two-solar-mass NS together with the analysis [23] of the data obtained by recent NASA telescope NICER measurements of x-ray emissions from the heaviest of the precisely known $2M_\odot$ PSR J0740+6620, which indicates that PSR J0740+6620 has a radius in the range of (11.4 - 16.1) km at the 68% credibility level, suggests that the SOS should be beyond the conformal limit [20, 24]. This trend may continue when future more precise measurements of masses, radii, and deformabilities of NS are obtained.

In this paper, we are interested in investigating the effect that a strong magnetic field can have on the SOS of both a hadronic and a quark cold-dense system, and in what it has to add to the question of the possible violation of the conformal limit. In doing so, it is important to consider that one of the consequences of the presence of a strong magnetic field that has been investigated in heavy-ion collisions [25], as well as in NS [5, 6, 26–28] is the modification of the system EOS that now become anisotropic (i.e. the system pressures along and transverse to the direction of the magnetic field are different). Since, the speed of sound in the medium is associated with oscillations in pressure, it is expected that the anisotropy in the pressure also affects the transmission of sound along and perpendicular to the field. Hence, we will investigate this phenomenon for two phases that can bring some light to the problem: the hadronic phase modeled by the Walecka model [29] and the quark phase described by the MIT Bag model [30]. We will work in the zero-temperature

(T=0) limit, thus our results will be in particular useful for NS applications where the T=0 limit is a good approximation since the baryonic chemical potential of the dense medium there is much larger than the temperature.

The paper is outlined as follows. In Sec. 2 we derive from first principles the anisotropic wavelike equation from where the longitudinal and transverse SOS in the presence of a uniform magnetic field can be extracted. We find that the anisotropic formulas relate the SOS with the stiffness of the anisotropic EOS in each corresponding direction. We then find in Sec. 3 the corresponding SOS in a hadronic phase characterized by the non-linear Walecka (NLW) model first, and then in a dense quark-matter medium described by the MIT bag model. In Sec. IV, we analyze numerically the characteristics of the SOS in each phase and specifically we investigate how they depend on the magnetic field. We show that in the strong-field limit while the transverse speed of sound approaches zero, the longitudinal component exceeds the conformal limit approaching the maximum value c. In Sec. V, we summarize the paper's main results and point out some possible future directions. In Appendix A, the details of the strong-field limit calculation are exposed.

II. THE SPEED OF SOUND IN THE PRESENCE OF A MAGNETIC FIELD

A. The equations of state in a magnetic field

We want to briefly introduce the anisotropic stress-energy tensor in the presence of a magnetic field from where the anisotropic EOS are obtained and from which the SOS are derived for a magnetized system. It is well known that the system EOS are derived from the quantum-statistical average of its stress-energy tensor. As has been stressed in Refs. [5, 26], the presence of a uniform magnetic field introduces a new symmetry breaking that is reflected in the covariant structures of the stress-energy tensor. Specifically, a uniform magnetic field along the third direction, x_3, breaks the rotational O(3) invariance making an explicit separation between the direction along the field lines and those which are transverse to them. Hence, in the presence of a medium (i.e. at finite density and/or temperature) that breaks Lorentz invariance, the magnetized medium exhibits a stress-energy tensor expanded in three independent structures

$$\tau^{\mu\nu} = a_1\eta^{\mu\nu} + a_2 u^\mu u^\nu + a_3 \widehat{F}^{\mu\rho}\widehat{F}^{\nu}_{\rho}, \tag{4}$$

where $\eta^{\mu\nu}$ is the Minkowski metric, u_μ is the medium four-velocity, which in the rest frame takes the value $u_\mu = (1, \overrightarrow{0})$, and $\widehat{F}^{\mu\rho} = F^{\mu\rho}/B$ is the normalized electromagnetic strength tensor.

The scalar coefficients a_i, $i = 1, 2, 3$ are found from the quantum-statistical average of the energy-momentum tensor,

$$\frac{1}{\beta V}\langle\hat{\tau}^{\mu\nu}\rangle = \Omega\eta^{\mu\nu} + (\mu\rho + TS)u^\mu u^\nu + BM\eta^{\mu\nu}_{\perp} \tag{5}$$

They are given in terms of the system thermodynamic potential Ω , the average particle-number density, $\rho = -(\partial\Omega/\partial\mu)_{V,T}$, the entropy, $S = -(\partial\Omega/\partial T)_{V,\mu}$, and the system magnetization $M = -(\partial\Omega/\partial B)_{V,T,\mu}$. In (5), V is the system volume, B is the magnetic field, μ is the chemical potential, $\beta = 1/T$ is the inverse absolute temperature and $\eta^{\mu\nu}_{\perp} = diag(0, -1, -1, 0)$.

From (5), we can find the system anisotropic EOS by calculating the different components of $\langle\hat{\tau}^{\mu\nu}\rangle$, which are given in terms of the energy density ε, parallel pressure $P_\parallel$ and perpendicular pressure $P_\perp$ as [5]

$$\varepsilon = \frac{1}{\beta V}\langle\hat{\tau}^{00}\rangle, \quad P_\parallel = \frac{1}{\beta V}\langle\hat{\tau}^{33}\rangle, \quad P_\perp = \frac{1}{\beta V}\langle\hat{\tau}^{\perp\perp}\rangle \tag{6}$$

As is known, for NS physics, since $\mu \gg T$, the $T = 0$ limit is a justified approximation and the EOS reduces to

$$\varepsilon = \Omega + \mu\rho + \frac{B^2}{2}, \tag{7}$$

$$P_{\parallel} = -\Omega - \frac{B^2}{2}, \quad P_{\perp} = -\Omega - MB + \frac{B^2}{2}. \tag{8}$$

In (7)-(8) the quadratic terms in B arise from the Maxwell contribution to the energy momentum tensor

$$\tau_M^{\mu\nu} = \frac{B^2}{2}\left(\eta_{\parallel}^{\mu\nu} - \eta_{\perp}^{\mu\nu}\right). \tag{9}$$

Since the EOS is the basis for the calculation of the SOS, the EOS anisotropy will be transferred to it as we will see as follows.

B. The Speed of Sound with Anisotropic Pressures

In an isotropic system the speed of sound squared (SOS^2) is known to be given by the differential slope of the P vs ε curve, $\partial P/\partial\varepsilon$. Due to the existence of a pressure anisotropy in the presence of a magnetic field, a corresponding anisotropy in the speed of sound is expected to exist. As follows we will show that the speed of sound becomes anisotropic and given by

$$V_{\parallel}^2 = \Big[\frac{\partial P_{\parallel}}{\partial\epsilon}\Big]_B, \qquad V_{\perp}^2 = \Big[\frac{\partial P_{\perp}}{\partial\epsilon}\Big]_B \tag{10}$$

where $V_{\parallel}$ and $V_{\perp}$ are the sound velocities along and perpendicular to the field direction, respectively.

Our goal now is to justify (10) from general principles. From the results (5), (7) and (8) we can express the quantum-statistical average of the stress-energy tensor as

$$\frac{1}{\beta V}\langle\hat{\tau}^{\mu\nu}\rangle = -P_{\parallel}\eta^{\mu\nu} + \left(\varepsilon + P_{\parallel}\right)u^{\mu}u^{\nu} + \left(P_{\parallel} - P_{\perp}\right)\eta_{\perp}^{\mu\nu}. \tag{11}$$

In (11), ε is the system energy density in a frame comoving with the fluid. In a general local Minkowski frame, where the fluid is moving with four velocity u_{μ}, the energy density is given by

$$\epsilon = -P_{\parallel} + \left(\varepsilon + P_{\parallel}\right)\gamma^2. \tag{12}$$

where $\gamma = [1 - v^2]^{-1/2}$ is the Lorentz factor and v is the magnitude of the system spatial velocity in the local Minkowski frame.

Assuming there are no external four forces, the hydrodynamics of the system is determined in the local Lorentz frame by the vanishing divergence of the stress-energy tensor, which is associated with the conservation of energy and linear momentum,

$$\partial_{\nu}\langle\hat{\tau}^{\mu\nu}\rangle = 0 \tag{13}$$

Substituting (11) into (13) and using (12) to simplify, (13) can can be broken into components as follows

$$\partial_0\epsilon + \nabla\cdot\left[(\epsilon + P_{\parallel})\vec{v}\right] = 0, \qquad \mu = 0, \tag{14}$$

$$\partial_\mu P_\perp + \partial_0 \left[(\epsilon + P_\parallel)v^\mu\right] + \partial_j \left[(\epsilon + P_\parallel)v^\mu v^j\right] = 0, \qquad \mu = 1, 2, \tag{15}$$

$$\partial_3 P_\parallel + \partial_0 \left[(\epsilon + P_\parallel)v^3\right] + \partial_j \left[(\epsilon + P_\parallel)v^3 v^j\right] = 0, \qquad \mu = 3 \tag{16}$$

where j is a spatial index. Using (14) to eliminate $\partial_0\epsilon$ from (15) and (16) we arrive at

$$(\epsilon + P_\parallel)\left[\partial_0 v^\mu + v^j \partial_j v^\mu\right] = -\partial_\mu P_\perp - v^\mu \partial_0 P_\parallel, \quad \mu = 1, 2 \tag{17}$$

$$(\epsilon + P_\parallel)\left[\partial_0 v^3 + v^j \partial_j v^3\right] = -\partial_3 P_\parallel - v^3 \partial_0 P_\parallel, \quad \mu = 3. \tag{18}$$

Now we consider a system that is at rest relative to a local Minkowski frame (i.e. with $v = 0$) and where ϵ, B, $P_\parallel$, and $P_\perp$ are uniform and constant throughout. Further, let the system be perturbed, $\epsilon \to \epsilon + \delta\epsilon$, $P_\parallel \to P_\parallel + \delta P_\parallel$, $P_\perp \to P_\perp + \delta P_\perp$, and in such a way that the fluid velocity in the local frame is also perturbed as $\vec{v} \to \delta\vec{v}$. Substituting these changes into (14), (17), and (18) and keeping terms to first order in the perturbation we get

$$\partial_0 \delta\epsilon + (\epsilon + P_\parallel)\partial_j(\delta v^j) = 0, \quad \mu = 0, \tag{19}$$

and

$$(\epsilon + P_\parallel)\partial_0 \delta v^\mu = -\partial_\mu \delta P_\perp, \qquad \mu = 1, 2, \tag{20}$$

$$(\epsilon + P_\parallel)\partial_0 \delta v^3 = -\partial_3 \delta P_\parallel, \quad \mu = i = 3. \tag{21}$$

Taking the time derivative of (19), the three divergence of (20) and (21), and combing the results we arrive at

$$\frac{\partial^2 \delta\epsilon}{\partial t^2} - \left(\frac{\partial^2}{\partial x^2} + \frac{\partial^2}{\partial y^2}\right)\delta P_\perp - \frac{\partial^2}{\partial z^2}\delta P_\parallel = 0. \tag{22}$$

Considering that ϵ, $P_\parallel$, and $P_\perp$ are in general functions of μ and B, the variations in ϵ, $P_\parallel$, and $P_\perp$ are given by

$$\begin{aligned} \delta\epsilon &= \frac{\partial\epsilon}{\partial\mu}\delta\mu + \frac{\partial\epsilon}{\partial B}\delta B, \\ \delta P_\parallel &= \frac{\partial P_\parallel}{\partial\mu}\delta\mu + \frac{\partial P_\parallel}{\partial B}\delta B, \\ \delta P_\perp &= \frac{\partial P_\perp}{\partial\mu}\delta\mu + \frac{\partial P_\perp}{\partial B}\delta B. \end{aligned} \tag{23}$$

In order to consider the response only to mechanical perturbations we take $\delta B = 0$ (taking $\delta B \neq 0$ would amount to a perturbation in the electromagnetic field), then (22) becomes

$$\frac{\partial\epsilon}{\partial\mu}\frac{\partial^2\delta\mu}{\partial t^2} - \frac{\partial P_\perp}{\partial\mu}\left(\frac{\partial^2}{\partial x^2} + \frac{\partial^2}{\partial y^2}\right)\delta\mu - \frac{\partial P_\parallel}{\partial\mu}\frac{\partial^2\delta\mu}{\partial z^2} = 0. \tag{24}$$

To identify (24) with a wave equation we define

$$V_\perp^2 = \frac{\partial P_\perp}{\partial \mu}\Big/\frac{\partial \epsilon}{\partial \mu} = \Big[\frac{\partial P_\perp}{\partial \epsilon}\Big]_B,\ V_\parallel^2 = \frac{\partial P_\parallel}{\partial \mu}\Big/\frac{\partial \epsilon}{\partial \mu} = \Big[\frac{\partial P_\parallel}{\partial \epsilon}\Big]_B \tag{25}$$

and arrive at an anisotropic wavelike equation

$$\frac{\partial^2 \delta\mu}{\partial t^2} - V_\perp^2\left(\frac{\partial^2}{\partial x^2} + \frac{\partial^2}{\partial y^2}\right)\delta\mu - V_\parallel^2 \frac{\partial^2}{\partial z^2}\delta\mu = 0. \tag{26}$$

Then, from (26), we see that $V_\parallel$ and $V_\perp$ describe in the local Minkowski frame the speeds of sound along and transverse to the magnetic field direction respectively. Furthermore, from (25) we see that their squares give the stiffness of the EOS in the two anisotropic directions.

As follows we calculate the speeds of sound for two magnetized phases that could be realized in the interior of NS: the hadronic and the quark dense phases in the presence of a magnetic field.

III. THE EOS OF DENSE MAGNETIZED PHASES

In this section, for the sake of completeness and to facilitate the reader's understanding, we summarize the results for the EOS of the hadronic and quark dense phases in the presence of a magnetic field. The results presented here will be the basis for calculating the speeds of sound in section IV.

A. The EOS of the Magnetized Dense Hadronic Phase

To describe magnetized hadronic matter we use the NLW model in a uniform background magnetic field $\vec{B} = B\hat{z}$. The Lagrangian density of the system can be expressed as a sum over its baryon (b), lepton (l), meson (m), and Maxwell (M) components

$$\mathcal{L}_H = \sum_b \mathcal{L}_b + \sum_l \mathcal{L}_l + \mathcal{L}_m + \mathcal{L}_M, \tag{27}$$

where

$$\begin{aligned}
\mathcal{L}_b &= \bar{\psi}_b\left(i\gamma_\mu\partial^\mu - q_b\gamma_\mu A^\mu + \gamma^0\mu_b - m_b + g_{\sigma b}\sigma - g_{\omega b}\gamma_\mu\omega^\mu - g_{\rho b}\tau_{3_b}\gamma_\mu\rho^\mu + ik_n\sigma_{\mu\nu}F^{\mu\nu}\delta_{nb}\right)\psi_b \\
\mathcal{L}_l &= \bar{\psi}_l\left(i\gamma_\mu\partial^\mu - q_l\gamma_\mu A^\mu + \gamma^0\mu_l - m_l\right)\psi_l \\
\mathcal{L}_m &= \frac{1}{2}\partial_\mu\sigma\partial^\mu\sigma - \frac{1}{2}m_\sigma^2\sigma^2 - U(\sigma) + \frac{1}{2}m_\omega^2\omega_\mu\omega^\mu - \frac{1}{4}\Omega^{\mu\nu}\Omega_{\mu\nu} + \frac{1}{2}m_\rho^2\rho_\mu\rho^\mu - \frac{1}{4}P^{\mu\nu}P_{\mu\nu} \\
\mathcal{L}_M &= -\frac{1}{4}F^{\mu\nu}F_{\mu\nu}.
\end{aligned} \tag{28}$$

Here τ_{3_b} denotes the baryon isospin projection operator and $g_{\sigma b}$, $g_{\omega b}$, and $g_{\rho b}$ are the baryon-meson couplings (refer to Table I). The mesonic and electromagentic field tensors are given by: $\Omega_{\mu\nu} = \partial_\mu\omega_\nu - \partial_\nu\omega_\mu$, $P_{\mu\nu} = \partial_\mu\rho_\nu - \partial_\nu\rho_\mu$, and $F_{\mu\nu} = \partial_\mu A_\nu - \partial_\nu A_\mu$, and the scalar self-interaction potential (see Table 1 for a list of parameter values) is given by

$$U(\sigma) = \frac{1}{3}cm_n(g_{\sigma N}\sigma)^3 + \frac{1}{4}d(g_{\sigma N}\sigma)^4. \tag{29}$$

In [6], it was found that for magnetized charged fermions, the magnetic field-anomolous magnetic moment (B-AMM) interaction does not significantly affect the systems EOS, so in $\mathcal{L}_b$ we only include the B-AMM interaction for the neutrons (indexed by $b = n$) via the last term in that expression. There, the neutron-anomalous magnetic moment (N-AMM) is given by $k_n = \mu_N g_N/2$, where $\mu_N = |e|\hbar/2m_p = 3.15 \times 10^{-18}$MeV/G is the nuclear magneton [33], m_p is the proton mass and g_N is the Landé g factor for the neutron. We consider a system with baryon content comprised only of neutrons and protons ($b = n, p$) and lepton content comprised only of electrons ($l = e$). The meson fields will be considered in the mean-field approximation (MFA), where only the expectation values $\bar{\sigma} = \langle\sigma\rangle$, $\bar{\omega}_0 = \langle\omega_0\rangle$, $\bar{\rho}_0 = \langle\rho^0\rangle$ contribute into the one-loop thermodynamic potential.

TABLE I: Saturation density ρ_0, Scalar, $g_{\sigma N}$, and vector meson-nucleon, $g_{\omega N}$, $g_{\rho N}$, couplings as well as meson self interaction coefficients, c, d, chosen to reproduce the binding energy, baryon density, symmetry energy coefficient and effective mass at nuclear saturation for a compression modulus $K = 30$, as reported in Ref. [34, 35].

$g_{\sigma N}$	$g_{\omega N}$	$g_{\rho N}$	c	d	ρ_0
8.910	10.610	8.196	.002947	-0.001070	.153fm^{-3}

The EOS for this system has been calculated in detail in Ref. [26]. Thus, we are only giving the results here.

$$\begin{aligned}
\varepsilon &= {\Omega_f}^H + \sum_i E_i^F \rho_i^H + \frac{B^2}{2} + \left\{\frac{1}{2}m_\sigma^2\bar{\sigma}^2 + U(\bar{\sigma}) + \frac{1}{2}m_\omega^2\bar{\omega}_0^2 + \frac{1}{2}m_\rho^2\bar{\rho}_0^2\right\},\\
P_\perp &= -{\Omega_f}^H - BM_f^H + \frac{B^2}{2} + \left\{-\frac{1}{2}m_\sigma^2\bar{\sigma}^2 - U(\bar{\sigma}) + \frac{1}{2}m_\omega^2\bar{\omega}_0^2 + \frac{1}{2}m_\rho^2\bar{\rho}_0^2\right\},\\
P_\parallel &= -{\Omega_f}^H - \frac{B^2}{2} + \left\{-\frac{1}{2}m_\sigma^2\bar{\sigma}^2 - U(\bar{\sigma}) + \frac{1}{2}m_\omega^2\bar{\omega}_0^2 + \frac{1}{2}m_\rho^2\bar{\rho}_0^2\right\},
\end{aligned} \tag{30}$$

where

$$\Omega_f^H = \Omega_n + \Omega_p + \Omega_e. \tag{31}$$

is the sum of the neutron, proton and electron one-loop thermodynamic potentials given respectively in the weak-field approximation by

$$\begin{aligned}
\Omega_n &= \frac{-1}{48\pi^2}\left\{2\left(\sqrt{1-\left(\frac{m_n^*+k_nB}{E_n^F}\right)^2} + (B\to -B)\right){E_n^F}^4\right.\\
&+ 4k_nB\left(\sin^{-1}\left[\frac{m_n^*+k_nB}{E_n^4}\right] - (B\to -B)\right)E_n^{F3}\\
&+ \left[(m_n^*+k_nB)^3(3m_n^*-k_nB)\left(\ln\left[1+\sqrt{1-\frac{m_n^*+k_nB}{E_n^F}}\right] - \ln\left|\frac{m_n^*+k_nB}{E_n^F}\right|\right) + (B\to -B)\right]\\
&+ \left.\left[\left(8k_nB(m_n^*+k_nB) - 5(m_n^*+k_nB)^2\right)\sqrt{1-\frac{m_n^*+k_nB}{E_n^F}} + (B\to -B)\right]\right\},
\end{aligned} \tag{32}$$

$$\Omega_p = \frac{-1}{24\pi^2}\left\{\left(2{E_p^F}^4 - 5{m_p^*}^2{E_p^F}^2\right)\sqrt{1-\left(\frac{m_p^*}{E_p^F}\right)^2} + \left(3{m_p^*}^4 + 2(eB)^2\right)\ln\left[\frac{E_p^F + \sqrt{{E_p^F}^2 - {m_p^*}^2}}{m_p^*}\right]\right\}, \tag{33}$$

$$\Omega_e = \frac{-1}{24\pi^2}\left\{\left(2{E_e^F}^4 - 5{m_e}^2{E_e^F}^2\right)\sqrt{1-\left(\frac{m_e}{E_e^F}\right)^2} + \left(3{m_e}^4 + 2\left(eB\right)^2\right)\ln\left[\frac{E_e^F + \sqrt{{E_e^F}^2 - {m_e}^2}}{m_e}\right]\right\}, \tag{34}$$

with $m_n^* = m_n - g_{\sigma N}\bar{\sigma}$, $m_p^* = m_p - g_{\sigma N}\bar{\sigma}$; $\rho_i^H = -\partial{\Omega_f}^H/\partial\mu_i$ are the i^{th} particle species number densities at zero temperature and finite density, which are given by

$$\begin{aligned}
\rho_n &= \frac{1}{3\pi^2}\left({E_n^F}^2 - {m_n^*}^2\right)^{\frac{3}{2}}, \\
\rho_p &= \frac{1}{3\pi^2}\left[\left({E_p^F}^2 - {m_p^*}^2\right)^{\frac{3}{2}} + \frac{(eB)^2}{4\sqrt{{E_p^F}^2 - {m_p^*}^2}}\right], \\
\rho_e &= \frac{1}{3\pi^2}\left[\left({E_e^F}^2 - m_e^2\right)^{\frac{3}{2}} + \frac{(eB)^2}{4\sqrt{{E_e^F}^2 - m_e^2}}\right],
\end{aligned} \tag{35}$$

E_i^F are the Fermi energies

$$E_n^F = \mu_n - g_{\omega N}\bar{\omega}^0 - g_{\rho N}\tau_{3_n}\bar{\rho}^0, \quad E_p^F = \mu_p - g_{\omega N}\bar{\omega}^0 - g_{\rho N}\tau_{3_p}\bar{\rho}^0, \quad E_e^F = \mu_e, \tag{36}$$

and $M_f^H = -\partial\Omega_f^H/\partial B$ is the system magnetization. In (35) we neglected the N-AMM contribution into ρ_n.

We will work under the assumption that the system is beta equilibriated

$$\mu_b = \mu_n, \quad \mu_p = \mu_n - \mu_e. \tag{37}$$

as well as neutral

$$\frac{\partial\Omega_f^H}{\partial\mu_e} = \rho_p - \rho_e = 0 \tag{38}$$

while taking into account the condensate solutions to the minimum equations

$$\frac{\partial\Omega^H}{\partial\bar{\sigma}} = \frac{\partial\Omega^H}{\partial\bar{\omega}_0} = \frac{\partial\Omega^H}{\partial\bar{\rho}_0} = 0. \tag{39}$$

In the approach under consideration we are working in the weak-field approximation (WFA) where the Landau sums were approximated using the Euler-Maclaurin formula (see the appendix of [6]) with order parameter (eB). To justify this, when working in the WFA we will use fields only up to 10^{18}G, in which case eB is still sufficiently small.

In section IV we will use the EOS (30) to numerically calculate the corresponding speed of sound of this phase for different parameter values.

B. The EOS of the Magnetized Dense Quark Phase

To describe the quark content we use the MIT bag model where the quarks are taken to be free inside of an effective "bag". The effects of the bag are formally realized in the model by adding (subtracting) a fixed constant to the energy density (pressure). We consider a system of up and down quarks, and electrons immersed in a uniform background magnetic field $\vec{B} = B\hat{z}$, which has Lagrangian density

$$\mathcal{L}^Q = \sum_q \mathcal{L}_q + \mathcal{L}_e + \mathcal{L}_M, \tag{40}$$

where

$$\mathcal{L}_q = \bar{\psi}_q \left(i\gamma_\mu \partial^\mu - q_q \gamma_\mu A^\mu + \mu_q \gamma^0 - m_q \right) \psi_q. \tag{41}$$

The quark index q runs over up and down flavors, u, d respectively, and is degenerate in the three color charges. We use for the current quark masses $m_u = m_d = 5.5$MeV and μ_q denotes the chemical potential of flavor q. In the WFA, the finite-density one-loop thermodynamic potential for each quark is arrived at by taking $m_e \to m_q$, $e \to q_q$, $\mu_e \to \mu_q$ in Ω_e, and multiplying by an overall factor of 3 to account for the color degeneracy. Hence, the fermion thermodynamic potential is

$$\Omega_f^Q = \Omega_u + \Omega_d + \Omega_e, \tag{42}$$

where

$$\begin{aligned}
\Omega_u &= \frac{-1}{8\pi^2} \left\{ \left(2{\mu_u}^4 - 5{m_u}^2{\mu_u}^2 \right) \sqrt{1 - \left(\frac{m_u}{\mu_u} \right)^2} + \left(3{m_u}^4 + \frac{8}{9} (eB)^2 \right) \ln \left[\frac{\mu_u + \sqrt{{\mu_u}^2 - {m_u}^2}}{m_u} \right] \right\}, \\
\Omega_d &= \frac{-1}{8\pi^2} \left\{ \left(2{\mu_d}^4 - 5{m_d}^2{\mu_d}^2 \right) \sqrt{1 - \left(\frac{m_d}{\mu_d} \right)^2} + \left(3{m_d}^4 + \frac{2}{9} (eB)^2 \right) \ln \left[\frac{\mu_d + \sqrt{{\mu_d}^2 - {m_d}^2}}{m_d} \right] \right\}, \\
\Omega_e &= \frac{-1}{24\pi^2} \left\{ \left(2{\mu_e}^4 - 5{m_e}^2{\mu_e}^2 \right) \sqrt{1 - \left(\frac{m_e}{\mu_e} \right)^2} + \left(3{m_e}^4 + 2 (eB)^2 \right) \ln \left[\frac{\mu_e + \sqrt{{\mu_e}^2 - {m_e}^2}}{m_e} \right] \right\}.
\end{aligned} \tag{43}$$

are respectively the u, d and electron one-loop thermodynamic potentials in the weak-field approximation.

After quantum-statistical averaging the EOS for the dense quark system are found to be

$$\begin{aligned}
\varepsilon &= \Omega_f^Q + \sum_{i=u,d,e} \mu_i \rho_i^Q + Bag, \\
P_\perp^Q &= -\Omega_f^Q - B M_f^Q + \frac{B^2}{2} - Bag, \\
P_\parallel^Q &= -\Omega_f^Q - \frac{B^2}{2} - Bag.
\end{aligned} \tag{44}$$

with $M_f^Q = -\partial \Omega^Q / \partial B$ being the quark system magnetization, and the quark number densities are given by

$$\begin{aligned}
\rho_u^Q &= \frac{1}{\pi^2} \left[\left({\mu_u}^2 - m_u^2 \right)^{\frac{3}{2}} + \frac{(eB)^2}{9\sqrt{{\mu_u}^2 - m_u^2}} \right], \\
\rho_d^Q &= \frac{1}{\pi^2} \left[\left({\mu_d}^2 - m_d^2 \right)^{\frac{3}{2}} + \frac{(eB)^2}{36\sqrt{{\mu_d}^2 - m_d^2}} \right].
\end{aligned} \tag{45}$$

The electron number density is the same as in (35).

We assume that the system is beta equilibriated

$$\mu_u = \frac{1}{3}\mu - \frac{2}{3}\mu_e, \quad \mu_d = \frac{1}{3}\mu + \frac{1}{3}\mu_e. \tag{46}$$

and neutral

$$\frac{\partial\Omega_f^Q}{\partial\mu_e} = \frac{2}{3}\rho_u - \frac{1}{3}\rho_d - \rho_e = 0 \tag{47}$$

In (46), μ is the baryonic chemical potential and μ_e the electric one.

The baryonic charge density is given by

$$\rho_b^Q = -\frac{\partial\Omega_f^Q}{\partial\mu} = \frac{1}{3}\rho_u + \frac{1}{3}\rho_d. \tag{48}$$

For the numerical calculations we will take Bag =(180MeV)^4 to be the value of the bag constant.

IV. THE SPEED OF SOUND IN THE HADRONIC VS QUARK PHASE

To find the SOS of the hadronic and quark phases we rely on the EOS (30) and (44) respectively. In the hadron system there are six independent parameters B, μ_n, μ_e, $\bar{\sigma}$, $\bar{\omega}_0$, and $\bar{\rho}_0$. Taking into account the neutrality condition (38) and the condensate equations (39), the number of independent parameters reduces to two. Finally, fixing B, the EOS becomes an implicit function of μ_n. Similarly, the quark system has three independent parameters B, μ, and μ_e. After considering the neutrality condition (47) they reduce to two, and by fixing the magnetic field, the EOS finally depends only on μ. We call attention that for hadrons, μ_n corresponds to their baryonic chemical potential.

The SOS^2 for each system can then be determined from the general expressions given in Eqs. (25). In Fig.1 the parallel and perpendicular SOS^2 as defined in (25) are plotted for both the hadron and quark systems at different values of the magnetic field. To compare both systems, we have plotted each SOS^2 versus the normalized baryonic density in units of the nuclear saturation density $\rho_0 = 0.153$ fm^{-3} and took into account that the quark deconfined phase should be realized at relatively higher densities (For instance in Ref. [26] it was found to take place at $\rho = 4\rho_0$.). The considered magnetic field values are concordant with the WFA for those densities.

From Fig. 1 we observe that the values of the SOS increase with the density for hadrons, as well as for quarks. This is a consequence of the competition between the fluid stiffness, which increases with density and the density itself which is expressed by the general Newton-Laplace formula $V_s = \sqrt{K_s/\rho}$, where K_s is the coefficient of stiffness (also called the elastic bulk modulus) and ρ the fluid density. That is, the increase in density produces an increase in K_s, which is larger than the effect of the medium's inertial increase measured by ρ itself in the Newton-Laplace formula. It is possible to give a second reading for the behavior of the SOS^2 with ρ in Fig.1. It is also indicating that both media increase their resistance to deformation with density, thus allowing the pressure perturbation to travel quicker without significant losses produced by the medium's deformation. The physical scenario we are discussing here for dense media is framed by the same principle that explains why the speed of sound is faster in solids than in liquids or gasses.

Another observation from Fig. 2 is that for hadrons the effect of the magnetic field is insignificant even up to field values of $\sim 10^{18}$ G independently of whether or not the interaction of the magnetic field with the N-AMM is taken into account. We should comment that when the interaction of the N-AMM with the magnetic field is included in the many-particle thermodynamic potential, it was found [36, 37] that for magnetic fields that exceed the Fermi energy ($\gtrsim 10^{18}$ G), the magnetic field contribution to the many-particle EOS becomes significant. That is, it was found in Refs. [36, 37], that at those fields a complete spin polarization of the neutrons occurs, resulting in an overall stiffening of the many-particle EOS that overwhelms the softening induced by Landau quantization of the proton and electron spectra. Thus, it should be expected that a similar effect is reflected in the system SOS. In Fig. 3 the effects of the magnetic field AMM interaction is considered at $\sim 10^{19}$ G over baryonic densities where both the electrons and protons are in their lowest Landau levels

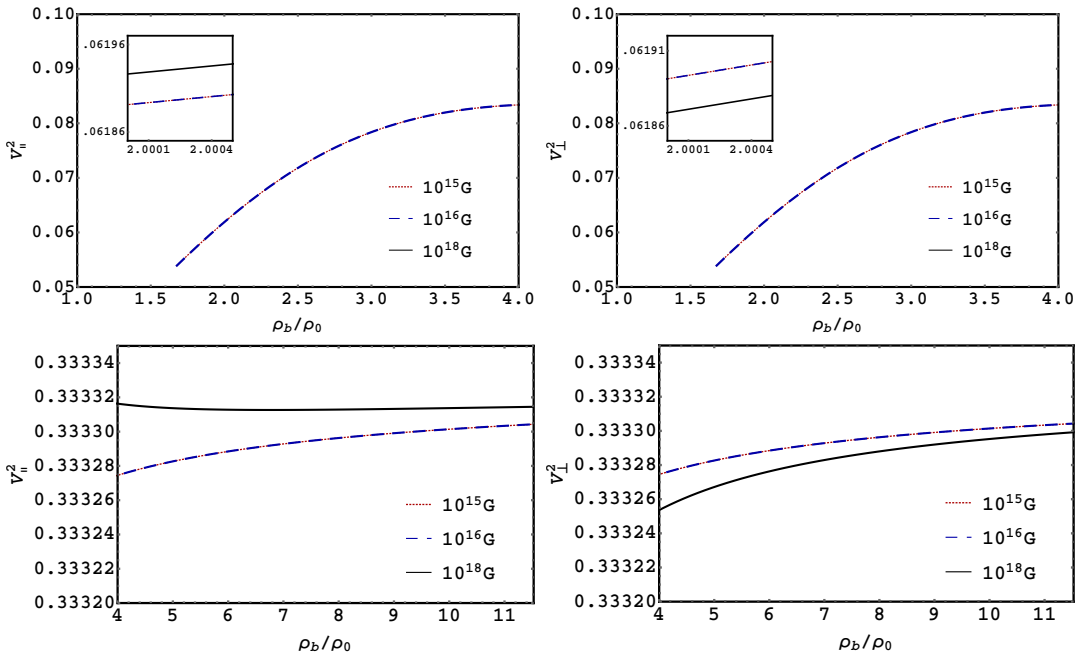

FIG. 1: (Color online) Parallel (**Left**) and Perpendicular (**Right**) SOS^2 in the hadron (**Upper**) and quark (**Lower**) systems versus normalized baryonic charge density ρ_b/ρ_0 at magnetic field strength values of 10^{15}G (red-dotted), 10^{16}G (blue-dashed), and 10^{18}G (black-solid; present in the inset of the hadron plots).

(LLL) (see Appendix B). But we should call attention to the fact that those fields will produce a negative parallel pressure when the Maxwell pressure is included as seen in Fig. 4, which will make the NS structure unstable under a large gravitational pull.

On the other hand, the SOS^2 in the magnetized hadronic system are well below the conformal limit and do not display a significant splitting between $V_\parallel$ and $V_\perp$. The fact that even at fields of $\sim 10^{18}$ G the SOS of the magnetized hadronic system is roughly the same in the longitudinal and transverse directions is indicating that the anisotropy produced by the magnetic field is not apparent in a system with very large hadronic masses. The field has to be larger than 10^{20} G to establish a quantum regime where the Landau quantization of the transverse momentum for protons becomes effective, as can be seen by equating the magnetic energy $\hbar\omega_c$, where $\omega_c = qB/mc$ is the cyclotron frequency in cgs units, to the corresponding rest-energy mc^2. Hence, the range of critical fields for different charged particles is quite wide. For example, for electrons, $B_c^{(e)} = 4.4 \times 10^{13}$ G, for quark matter formed by u and d quarks with current masses $m_u = m_d = 5$ MeV$/c^2$, it is $B_c^{(u,d)} = 10^2 B_c^{(e)} = 4.4 \times 10^{15}$ G and for protons, whose mass is 938 MeV$/c^2$, one finds $B_c^{(p)} = 1.6 \times 10^{20}$ G.

For quarks, the effect of the magnetic field even at $\sim 10^{18}$ G is not significant for the range of considered densities, as seen from Fig. 1. There, the AMM effect does not effectively change the result, since for charged fermions the AMM effect on the EOS turns insignificant [6]. It should also be noticed that, while the magnetic field increases $V_\parallel$, it decreases $V_\perp$. This dual effect can be understood from the fact that increasing the field the gap between Landau levels increases and consequently confining the quarks to the lowest Landau levels. Then, while the fluid becomes more compact and therefore facilitating the sound propagation along the field lines, it makes the propagation in the transverse direction more difficult, since the Landau quantization hinders the

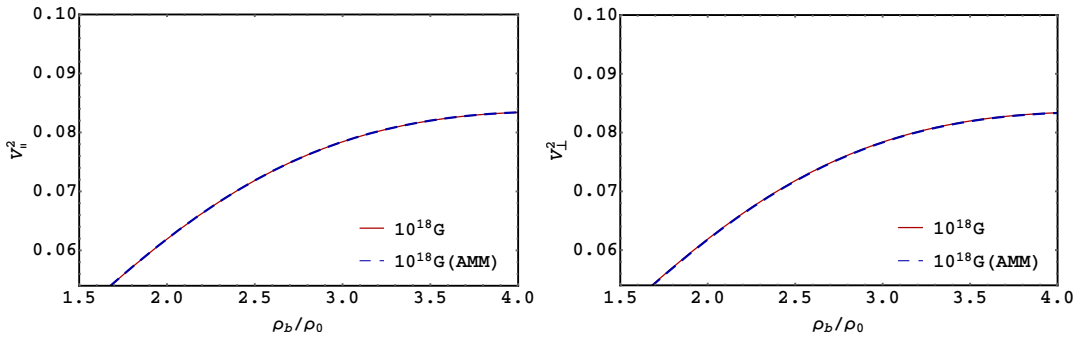

FIG. 2: (Color online) Parallel (a) and Perpendicular (b) SOS^2 in the hadron system versus normalized baryonic charge density ρ_b/ρ_0 at 10^{18}G with the contribution of the B-AMM interaction (blue-dashed) and without that contribution (red-dotted).

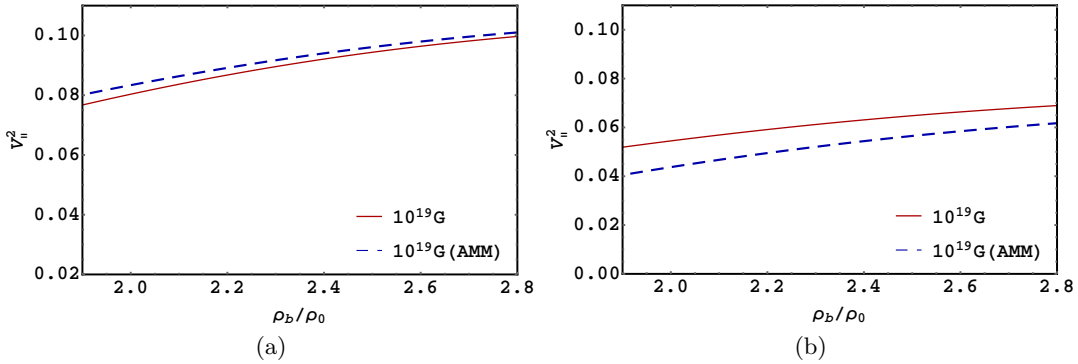

FIG. 3: (Color online) Parallel (a) and Perpendicular (b) SOS^2 in the hadron system versus normalized baryonic charge density ρ_b/ρ_0 at 10^{19}G with the contribution of the B-AMM interaction (blue-dashed) and without that contribution (red-dotted).

transverse wave propagation. This can be clearly seen looking to an extreme situation as we did in Appendix A where it was considered the strong-field limit, which completely confines the quarks into the LLL. In Appendix A, it was shown that in the LLL-approximation $V_\perp = 0$, indicating that if the charged particles are isolated into the LLL, no perturbation can be transmitted along the transverse direction (i.e. there is no medium to transmit the sound perturbation). On the contrary, as seen from Fig. 5, $V_\parallel^2$ is above the conformal limit and even reaches the causal limit $V_\parallel \approx 1$ at fields $B \simeq 10^{20}$ G. We call attention to the fact that the strong splitting between $V_\parallel$ and $V_\perp$ is another indication of the large anisotropy that can be generated by strong fields as was shown in other quark phases through their corresponding EOS [27, 38].

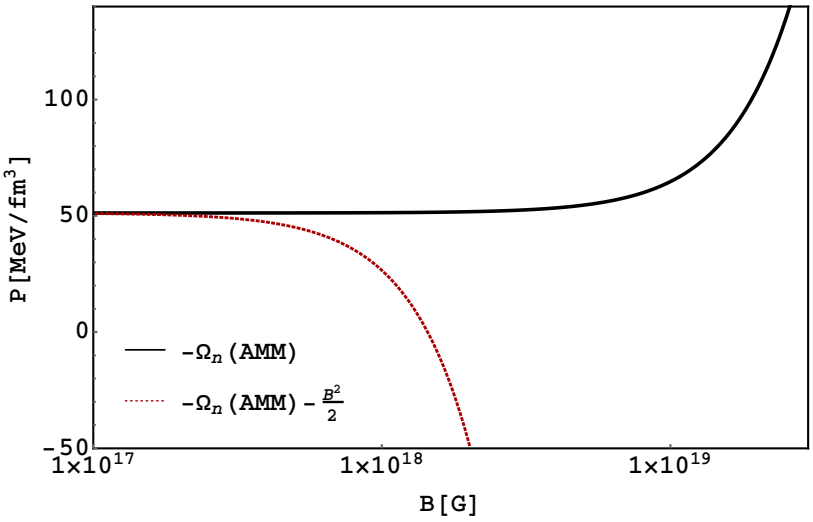

FIG. 4: Parallel pressure arising from the neutron component of the free energy versus magnetic-field with and without the Maxwell contribution.

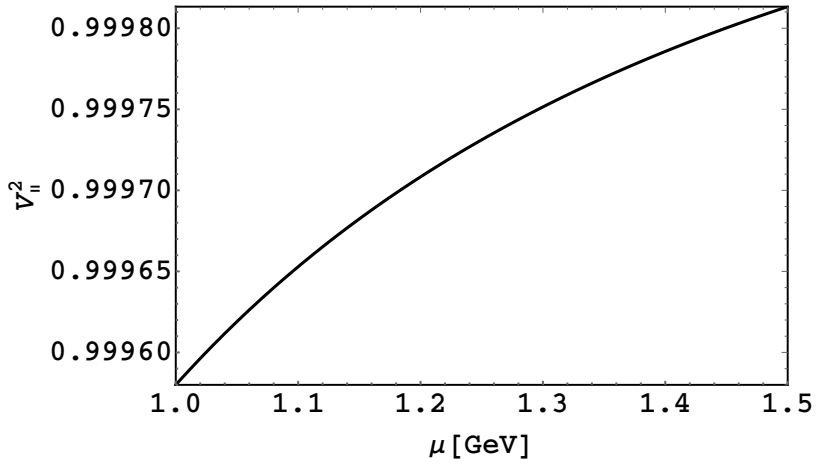

FIG. 5: Square of the parallel SOS versus baryonic chemical potential for dense quark matter in the LLL limit at $B = 10^{20}$G.

V. CONCLUDING REMARKS

An important outcome of our investigation is the reported anisotropy in the speed of sound. In the magnetized medium, the speed of sound is split with different values along and transverse to the magnetic field direction. In the quark phase, the speed of sound is larger than in the hadronic phase reaching at moderate fields a square value close to the conformal limit $\sim 1/3$, while in the hadronic phase it is smaller than that value. For the model under consideration the splitting is not too noticeable at moderate field values, since it depends on the pressure splitting which is apparent only for fields larger than 10^{18} G [5, 27]. On the contrary, we found that in the strong field limit,

when $B \gtrsim \mu^2$, the transverse speed velocity approaches zero, indicating that when the quarks are confined into the LLL there is no medium available to transmit a pressure perturbation in that direction; while in this limit the speed of sound along the field direction reaches the causal limit $V_{\parallel} \approx 1$, which is an indication of the large increase of the fluid stiffness along the field lines.

Since the SOS is a measure of the stiffness of the EOS, the fact that the magnetized quark matter phase has a larger speed of sound than the magnetized hadronic phase, indicates that a star with a magnetized quark phase can reach a larger mass. This result is in agreement with a recent finding [31] showing that the heaviest neutron stars, with masses $\sim 2M_{\odot}$, should have deconfined quark-matter in their cores.

We expect that other more realistic quark phases that can be realized at moderate densities, such as the magnetic dual chiral density wave (MDCDW) phase [39, 40], where the magnetization has an anomalous component that is linearly dependent on the baryonic chemical potential (i.e. $\Omega_{anom} \sim \mu b B$, where b is the modulation of the inhomogeneous chiral condensate in that phase), can produce a more significant anisotropy, since while the perpendicular velocity will not depend on the anomalous contribution, as is easy to check, the parallel velocity will be proportional to it. The modulation b in the region of interest is of the order of μ [39]. This anomalous term, which mixes B with a linear power of μ is possible thanks to the breaking of the parity symmetry by the inhomogeneous chiral condensate that allows for a term in the thermodynamic potential proportional to a Lorentz scalar depending on the totally antisymmetric Levi-Civita tensor, $\epsilon_{\mu\nu\rho\lambda}$, which can be contracted with the medium four velocity u_{ρ}, the magnetic field given through $F_{\mu\nu}$ and the modulation vector b_{λ}.

We should underline that since the SOS gives a measure of the stiffness of the EOS, which is in turn related through the TOV equations to how large the NS mass can be, the degree of anisotropy found in the SOS^2 for a given model at a certain strong field value, will be an indication of the necessity to modify the TOV equations to make possible the description of systems with cylindrical instead of spherical symmetry. Only with the appropriate modified TOV equations which are in agreement with the anisotropy in the pressures will we be sure about the effect a strong magnetic field can have on the mass-radius relationship. This is an open non-trivial question that needs to be accomplished.

Appendix A: Magnetized quark matter SOS in the strong-field approximation

In [26] the zero temperature many-particle thermodynamic potential per charged fermion species (indexed by "i") was found to be

$$\Omega_i = -g_i e_i B \int_{-\infty}^{\infty} \frac{dp_3}{(2\pi)^2} \left\{ \left(\mu_i - E_i\left(l=0\right)\right) \Theta\left(\mu_i - E_i\left(l=0\right)\right) + 2\sum_{l=1}^{\infty} \left(\mu_i - E_i\right) \Theta\left(\mu_i - E_i\right) \right\}, \tag{A1}$$

where $E_i = \sqrt{p_3^2 + 2e_i B l + m_i^2}$, with $l = 0, 1, 2, \cdots$ denoting the Landau level numbers and μ_i being the quark chemical potential for each flavor i and g_i being the degeneracy factor, $g_i = 3$, for quarks (i.e. corresponding to the color number $N_c = 3$) and $g_i = 1$ for electrons. The Heaviside functions induce cutoffs in both the p_3 integral and the sum over l. Performing the momentum integrals we get

$$\begin{aligned} \Omega_i = &- \frac{g_i e_i B}{(2\pi)^2} \left[\mu_i \sqrt{\mu_i^2 - m_i^2} - m_i^2 \ln \left| \frac{\mu_i + \sqrt{\mu_i^2 - m_i^2}}{m_i} \right| \right. \\ &\left. + 2\sum_{l=1}^{l_{max}} \left\{ \mu_i \sqrt{\mu_i^2 - \left(2e_i B l + m_i^2\right)} - \left(2e_i B l + m_i^2\right) \ln \left| \frac{\mu_i + \sqrt{\mu_i^2 - \left(2e_i B l + m_i^2\right)}}{\sqrt{2e_i B l + m_i^2}} \right| \right\} \right], \end{aligned} \tag{A2}$$

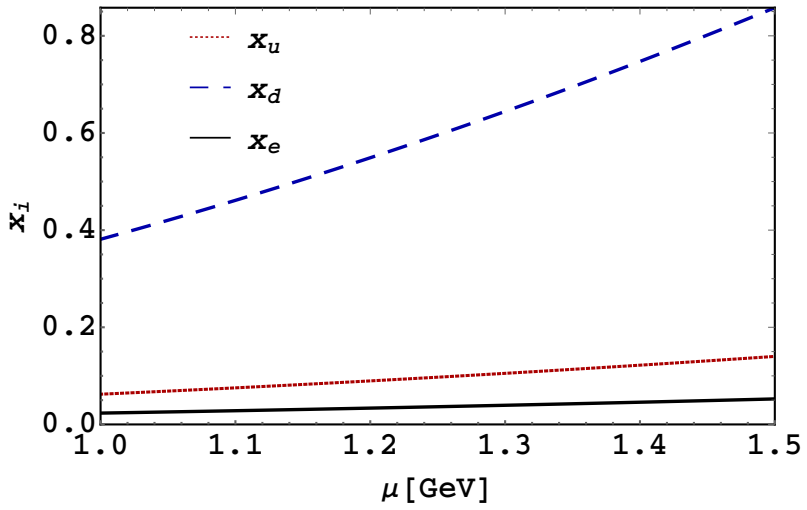

FIG. 6: (Color online) Argument of the maximum Landau level condition (A3) versus baryonic chemical potential per particle species (u quarks-red-dotted, d quarks-blue-dashed, electrons-black-solid).

where

$$l_i^{max} = \lfloor x_i \rfloor, \quad x_i = \frac{\mu_i^2 - m_i^2}{2e_i B}. \tag{A3}$$

From this last relation we see that when $e_i B > \mu_i^2$ the sum over Landau levels in Ω_i collapses leaving only the lowest Landau level (LLL) term. For magnetic fields satisfying this condition we have

$$\Omega_i^{LLL} = -\frac{g_i e_i B}{(2\pi)^2}\left[\mu_i\sqrt{\mu_i^2 - m_i^2} - m_i^2 \ln\left|\frac{\mu_i + \sqrt{\mu_i^2 - m_i^2}}{m_i}\right|\right]. \tag{A4}$$

Hence, the one-loop thermodynamic potential at $T = 0$ for the system of quarks considered in Sec. (III B) in the high-magnetic-field limit is given by

$$\Omega_f^Q = \Omega_u^{LLL} + \Omega_d^{LLL} + \Omega_e^{LLL}, \tag{A5}$$

where μ_u and μ_d are given in (46). Since each term in (A5) is proportional to B via (A4), we have that $M = -\Omega_f^Q/B$. From this, along with (8), we have that $P_\perp = B^2/2$ and so $V_\perp^2$ vanishes according to (25). On the other hand, the parallel SOS^2 is given by

$$V_\parallel^2 = \frac{e_u\sqrt{\left(\frac{1}{3}\mu - \frac{2}{3}\mu_e\right)^2 - m_u^2} + e_d\sqrt{\left(\frac{1}{3}\mu + \frac{1}{3}\mu_e\right)^2 - m_d^2}}{\frac{e_u\left(\frac{1}{3}\mu - \frac{2}{3}\mu_e\right)^2}{\sqrt{\left(\frac{1}{3}\mu - \frac{2}{3}\mu_e\right)^2 - m_u^2}} + \frac{e_d\left(\frac{1}{3}\mu + \frac{1}{3}\mu_e\right)^2}{\sqrt{\left(\frac{1}{3}\mu + \frac{1}{3}\mu_e\right)^2 - m_d^2}}}. \tag{A6}$$

To guarantee that the system is in the LLL at a given magnetic field, we must choose a baryonic chemical potential μ small enough that l^{max} in (A3) vanishes for each particle species. We will consider a reference magnetic field of $B_r = 10^{20}$G. The corresponding conditions are

$$x_u = \frac{\left(\frac{1}{3}\mu - \frac{2}{3}\mu_e\right)^2 - m_u^2}{2e_u B_r} < 1, \quad x_d = \frac{\left(\frac{1}{3}\mu + \frac{1}{3}\mu_e\right)^2 - m_d^2}{2e_d B_r} < 1, \quad x_e = \frac{\mu_e^2 - m_e^2}{2eB_r} < 1. \tag{A7}$$

Fig. 5 and Fig. 6 were constructed by imposing neutrality condition (at a field strength of $B = 10^{20}$ G; from which μ_e is determined for a given value of μ. Fig. 6 shows that the LLL assumption is valid according to (A7) for the values of μ being considered. In Fig. 5 the parallel SOS^2 given by (A6) can be seen to be much larger than $c^2/3$.

Appendix B: Magnetized hadron matter SOS in the strong-field approximation

In the hadron phase the electron and proton thermodynamic potentials in the LLL are given by (A4), where the electron component is the same as in (A5) and for the protons $g_i = 1$, $e_q = e_i$, $m_i = m_p^*$, and $\mu_i = \mu_p^*$. The fermionic thermodynamic potential in the hadron phase is given by

$$\Omega_f^H = \Omega_n + \Omega_p^{LLL} + \Omega_e^{LLL}. \tag{B1}$$

From (25) we find the hadron SOS^2 to be

$$V_\parallel^2 = \frac{\rho_n + \rho_p}{\mu_n \frac{\partial \rho_n}{\partial \mu_n} + \mu_p \frac{\partial \rho_p}{\partial \mu_n}}, \tag{B2}$$

$$V_\perp^2 = \frac{\rho_n - B\frac{\partial M_n}{\partial \mu_n}}{\mu_n \frac{\partial \rho_n}{\partial \mu_n} + \mu_p \frac{\partial \rho_p}{\partial \mu_n}}. \tag{B3}$$

Unlike the quark phase the perpendicular SOS^2 is nonzero, which is due to the fact the neutron component of the perpendicular pressure is dependent on μ_n. To enesure that the system is in the LLL we have from (A7) with $i = p$, that

$$x_p = \frac{\mu_p^{*2} - m_p^{*2}}{2eB} < 1, \quad x_e = \frac{\mu_e^2 - m_e^2}{2eB} < 1, \tag{B4}$$

where $M_n = -\partial\Omega_n/\partial B$ is the neutron magnetization. In Fig. 3, values of μ_n were chosen to ensure, via ($B4$), that the electron and proton components of the thermodynamic potential were in the LLL at 10^{19}G.

Acknowledgments

This work was supported in part by NSF grant PHY-2013222.

[1] V. Skokov, A.Yu. Illarionov and V. D. Toneev, Int. J. Mod. Phys. A24 (2009) 5925; V. Voronyuk, et al., Phys. Rev. C 83 (2011) 054911; A. Bzdak and V. Skokov, Phys. Lett. B 710, (2012) 171; L. Ou and B. A. Li, Phys. Rev. C 84, (2011) 064605; W. T. Deng and X. G. Huang, Phys. Rev. C 85, (2012) 044907, J. Bloczynski, X. G. Huang, X. Zhang and J. Liao, Phys. Lett. B 718, (2013) 1529; J. Bloczynski, X. G. Huang, X. Zhang and J. Liao, Nucl. Phys. A 939, (2015) 85.

[2] M. A. Livingstone and V. M. Kaspi, Astrophys. J 742 (2011) 31.
[3] A. Tiengo, P. Esposito, S. Mereghetti, R. Turolla, L. Nobili, F. Gastaldello, D. Gotz, G. L. Israel, N. Rea, L. Stella, et al. Nature 500 (2013) 312.
[4] L. Dong, S. L. Shapiro, Astrophys. J. 383 (1991) 745.
[5] E. J. Ferrer, V. de la Incera, J. P. Keith, I. Portillo, and P. L. Springsteen, Phys. Rev. C 82 (2010) 065802.
[6] E. J. Ferrer, V. de la Incera, D. Manreza Paret, A. Perez Martinez, and A. Sanchez, Phys. Rev. D 91 (2015) 085041.
[7] D. E. Kharzeev, Prog. Part. Nucl. Phys. 75 (2014) 133; E. J. Ferrer and V. de la Incera, Eur. Phys. J. A 52 (2016) 266.
[8] P. Demorest et al., Nature 467 (2010) 1081; Z. Arzoumanian, et al. Astrophys. J. Suppl. 235 (2018) 37.
[9] J. Antoniadis et al., Science 340 (2013) 6131.
[10] B. P. Abbott et al., Phys. Rev. Lett. 119 (2017) 161101; B. P. Abbott et al., Astrophys. J. Lett. 848 (2017) L13.
[11] O. Lourenco, C. H. Lenzi, M. Dutra, E. J. Ferrer, V. de la Incera, L. Paulucci, and J. E. Horvath, Phys. Rev. D 103, 103010 (2021).
[12] B. P. Abbott et al., Phys. Rev. X 9 (2019) 011001.
[13] J. Abadie et al., Classical Quantum Gravity 27 (2010) 173001.
[14] S. Borsanyi, G. Endrodi, Z. Fodor, et al. JHEP, 1208 (2012) 053.
[15] Ya. B. Zeldovich, Zh. Eksp. Teor. Fiz. 41 (1961) 1609; S. A. Bludman and M. A. Ruderman, Phys. Rev. 170 (1968) 1176; J. B. Hartle, Phys. Reports 46 (1978) 201; Y. B. Zeldovich and I. D. Novikov, Stars and Relativity, Dover Books on Physics (Dover Publications, 2014).
[16] S. Carignano, L. Lepori, A. Mammarella, M. Mannarelli, and G. Pagliaroli, Eur. Phys. J. A 53 (2017) 35.
[17] S. Hands, S. Kim, and J-I. Skullerud, Eur. Phys. J. C 48 (2006) 193.
[18] C. Hoyos, N. Jokela, D. RodrÃguez FernÃ¡ndez, and A. Vuorinen, Phys. Rev. D 94 (2016) 106008; C. Ecker, C. Hoyos, N. Jokela, D. RodrÃguez FernÃ¡ndez, and A. Vuorinen, JHEP 11 (2017) 031; A. Anabalon, T. Andrade, D. Astefanesei, and R. Mann, Phys. Lett. B 781 (2018) 547; P. M. Chesler, N. Jokela, A. Loeb, and A. Vuorinen, Phys. Rev. D 100 (2019) 066027.
[19] T. Gorda and P. Romatschke, Phys. Rev. D 92 (2015) 014019; Y. Fujimoto and K. Fukushima, Phys. Rev. D 105 (2022) 014025.
[20] I. Tews, J. Carlson, S. Gandolfi, S. Reddy, Astrophys.J. 860 (2018) 149.
[21] L. McLerran and S. Reddy, Phys. Rev. Lett. 122 (2019) 122701; K. S. Jeong, L. McLerran, and S. Sen, Phys. Rev. C 101 (2020) 035201; T. Zhao and J. M. Lattimer, Phys. Rev. D 102, (2020) 023021; J. Margueron, H. Hansen, P. Proust, and G. Chanfray, Phys. Rev. C 104, (2021) 055803; D. C. Duarte, S. Hernandez-Ortiz, K. Sang Jeong, and L. D. McLerran, Phys. Rev. D 104, L091901.
[22] D. B. Blaschke, D. Gomez Dumm, A. G. Grunfeld, T. Klahn, and N. N. Scoccola, Phys. Rev. C 75 (2007) 065804; M. G. Alford, S. Han, and M. Prakash, Phys. Rev. D 88 (Oct, 2013) 083013; J. Zdunik and P. Haensel, Astron. Astrophys. 551 (2013) A61; N. Chamel, A. Fantina, J. Pearson, and S. Goriely, Astron.Astrophys. 553 (2013) A22; A. Ayriyan, D. E. Alvarez-Castillo, D. Blaschke, H. Grigorian, and M. Sokolowski, Phys. Part. Nucl. 46 (2015), no. 5 854. T. Kojo, P. D. Powell, Y. Song, and G. Baym, Phys. Rev. D 91 (2015) 045003; G. Baym, S. Furusawa, T. Hatsuda, T. Kojo, and H. Togashi, Astrophys. J. 885 (2019) 42; J. R. Stone, V. Dexheimer, P. A. M. Guichon, and A. W. Thomas, MNRS, 502, 3476 (2021); M. Leonhardt, M. Pospiech, B. Schallmo, J. Braun, C. Drischler, K. Hebeler, and A. Schwenk, Phys. Rev. Lett. 125 (2020) 142502; K. B. Fadafan, J. Cruz Rojas, and N. Evans, Phys. Rev. D 101 (2020) 126005; G. Malfatti, M. G. Orsaria, I. F. Ranea-Sandoval, G. A. Contrera, and F. Weber, Phys. Rev. D 102 (2020) 063008; A. Li, Z. Y. Zhu, E. P. Zhou, J. M. Dong, J. N. Hu, and C. J. Xia, JHEAp 28 (2020) 19; Z. Roupas, G. Panotopoulos, and I. Lopes, Phys. Rev. D 103 (2021) 083015; A. Ayriyan, D. Blaschke, A. G. Grunfeld, D. Alvarez-Castillo, H. Grigorian, and V. Abgaryan, Eur. Phys. J. A 57, 318 (2021); C. Xia, Z. Zhu, X. Zhou, and A. Li, Chin. Phys. C 45 (2021) 055104; R. D. Pisarski, Phys. Rev. D 103, (2021) 071504; S. Pal, G. Kadam, and A. Bhattacharyya, arXiv:2104.08531 [hep-ph]; T. F. Motta, P. A. M. Guichon, and A. W. Thomas, Nucl. Phys. A 1009 (2021) 122157; Y-L. Ma and M. Rho, arXiv:2104.13822 [nucl-th]; M. Hippert, E. S. Fraga, J. Noronha, Phys .Rev.D 104 (2021) 034011.
[23] M. C. Miller et al., Astrophys. J. Lett. 918 (2021) L28; T. E. Riley et al., Astrophys. J. Lett. 918 (2021) L27.
[24] I. C. Drischler, S. Han and S. Reddy, arXiv: 2110.14896 [nucl-th].

[25] A. Shukla, Nucl.Phys.B 968 (2021) 115442; U. Gursoy, M. Jarvinen, G. Nijs, J. F. Pedraza, JHEP 03 (2021) 180; I. Ya. Aref'eva, K. Rannu, P. Slepov, "Energy Loss in Holographic Anisotropic Model for Heavy Quarks in External Magnetic Field" arXiv: 2012.05758 [hep-th].
[26] E. J. Ferrer and A. Hackebill, Hadron-Quark Phase Transition at Finite Density in the Presence of a Magnetic Field: Anisotropic Approach.
[27] L. Paulucci, E. J. Ferrer, V. de la Incera, and J. E. Horvath, Phys. Rev. D 83 (2011) 043009
[28] D. Deb, B. Mukhopadhyay , F. Weber, Astrophys.J. 922 (2021) 149; S. Das, K. N. Singh, L. Baskey, F. Rahaman, A. K. Aria, Gen. Rel. Grav. 53 (2021) 25.
[29] B. D. Serot and J. D. Walecka, Adv. Nucl. Phys. 16 (1986) 1.
[30] A. Chodos, R. L. Jaffe, K. Johnson, C. B. Thorn, and V. F. Weisskopf. Phys. Rev. D, 9 (1974) 3471; L. Paulucci, E. J. Ferrer, J. E. Horvath, V. de la Incera, J. Phys. G 40 (2013) 125202.
[31] E. Annala, T. Gorda, A. Kurkela, J. Nattila and A. Vuorinen, Nature Physics **16** (2020) 907, and extended data.
[32] M. G. Alford, S. Han and M. Prakash, Phys. Rev. D 88 (2013) 083013; P. Bedaque and A. W. Steiner, Phys. Rev. Lett. 114 (2015) 031103; M. G. Alford, G. F. Burgio, S. Han, G. Taranto and D. Zappala, Phys. Rev. D 92 (2015) 083002.
[33] J. Beringer, et al. (Particle data Group). Review of Particle Physics. Phys. Rev. D 86 (2012) 010001.
[34] A. Rabhi, H. Pais, P. K. Panda and C. Providencia, J. Phys. G: Nucl. Paet. Phys. 36 (2009) 115204;
[35] N. K. Glendenning and S. A. Moszkowski, Phys. Rev. Lett. 67 (1991) 2414.
[36] E. J. Ferrer and A. Hackebill, Phys. Rev. C 99 (2019) 065803.
[37] A. Broderick, M. Prakash,and J. M. Lattimer, Astrophys. J. 537 (2000) 351.
[38] S. Carignano, E. J. Ferrer, V. de la Incera, and L. Paulucci, Phys. Rev. D **92** (2015) 105018.
[39] I. E. Frolov, V. Ch. Zhukovsky and K. G. Klimenko, Phys. Rev. D 82 (2010) 076002.
[40] T. Tatsumi, K. Nishiyama and S. Karasawa, Phys. Lett. B 743 (2015) 66; E. J. Ferrer and V. de la Incera, Phys. Lett. B 769 (2017) 208; E. J. Ferrer and V. de la Incera, Nucl. Phys. B931 (2018) 192; Universe 4 (2018) 54; B. Feng, E. J. Ferrer, I. Portillo, Phys. Rev. D 101 (2020) 056012; (see for a review: E. J. Ferrer and V. de la Incera, Universe 7 (2021) 458).